PHYSICAL REVIEW B VOLUME 50, NUMBER 15 15 OCTOBER 1994-I

Adatom yields, sputtering yields, and damage patterns of single-ion impacts on Pt(111)

Thomas Michely and Christian Teichert*

Institut für Grenzflächenforschung und Vakuumphysik, Forschungszentrum Jülich, D-52425 Jülich, Germany

(Received 2 February 1994; revised manuscript received 2 June 1994)

Scanning-tunneling-microscopy methods are presented, which allow us to determine the adatom yield, the number of adatoms created per primary ion, and the sputtering yield. The reliability and the possible errors of the scanning-tunneling-microscope yield-determination methods are analyzed. For noble-gas ions normally incident on Pt(111), the dependence of adatom and sputtering yields on ion energy and ion mass are determined. The dependence of the adatom yield on these quantities is not in agreement with previous theoretical predictions. Possible mechanisms for the observed ion-energy and ion-mass dependence of the adatom yield are suggested. The observation of the damage patterns of single keV ion impacts and the lateral distribution of the damage features gives additional information on the damage mechanism.

I. INTRODUCTION

The creation of adatoms on a surface due to energetic ion impacts has been predicted theoretically by Webb and Harrison[1] in 1983. In a molecular-dynamics simulation of 5-keV Ar^+-ion bombardment of Cu(100) they observed a large number of atoms being pushed onto the outermost surface layer within a few picoseconds after the ion impact. This effect of target adatom creation was demonstrated experimentally in 1991.[2] After 600-eV Ar^+-ion bombardment of Pt(111) scanning-tunneling-microscopy (STM) topographs exhibited small monolayer-high Pt-adatom islands on the original surface layer. The presence of these adatom islands is a result of the nucleation of the target adatoms generated by the ion bombardment. Meanwhile, also on Cu(100) adatom generation due to ion bombardment has been observed, by Breemann and Boerma[3] with low-energy ion scattering and by Girard *et al.* with STM.[4] Adatom production on Cu(100) for ion energies even below the sputtering threshold has been predicted theoretically from molecular-dynamics simulations by Karetta and Urbassek.[5] Large amounts of adatoms per impact are predicted by Ghaly and Averback[6] for 10-keV Au on Au(100). Recently, we reported briefly on STM topographs of the Pt(111) surface damaged by single 5-keV Xe^+-ion impacts, which give evidence for large amounts of adatoms created by single impacts.[7] The deeper understanding of the adatom generation is highly desirable, both from a fundamental and an applied point of view. The sputtering yield has been for a long time the only observable to describe the ion-surface interaction. The adatom yield—the number of adatoms created per ion impact on the surface—is also a quantity which allows us to characterize this interaction, and it becomes an observable by the methods presented in this paper. Similar to the sputtering yield, the energy and projectile dependence should allow to test models for adatom generation and to elucidate the underlying atomic mechanisms. Ion-beam assisted deposition is nowadays a powerful technique to engineer thin films with specific properties.[8] The poor understanding of the effect of the applied ion beam on the atomic level is in sharp contrast to the technological importance of the method. One of the effects of the ion beam is obviously the adatom generation. It supplies additional diffusing species to the film surface. Moreover, the adatom yield should allow us to characterize on atomic scale the capability of the ion beam to mix atoms between the topmost layers of the growing film.

In this paper, we describe experiments and results of a systematic STM investigation of the projectile mass and energy dependence of the adatom yield and sputtering yield on Pt(111). These quantitative results on the yields are supplemented by the analysis of damage patterns of single-ion impacts.

II. EXPERIMENT

The experiments described in this paper have been performed in an apparatus designed for temperature-dependent STM investigations of ion bombardment effects. The apparatus is described in detail in Ref. 9. In principle, the sample is mounted thermally insulated but mechanically stiff to a solid metal block, which is damped against vibrations. The assembly is contained in a rigid manipulator tube with two degrees of freedom: rotation and translation. This allows the sample to be moved in front of the measuring stages: low-energy electron diffraction, Auger-electron spectroscopy, ion source, and STM.

The sample is heated by electron bombardment and can be cooled down to 120 K by a liquid-nitrogen heat-exchanger coupled via a copper braid to the sample. The temperature is controlled by a thermocouple spotwelded to the sample. A unique feature of the apparatus is the capability of the STM to operate in the wide temperature range between 120 and 450 K. The STM is a modified beetle-type STM[10] turned upside down, so that the micro-

0163-1829/94/50(15)/11156(11)/$06.00

scope is lowered onto the sample and not vice versa. All topographs presented were obtained under constant current imaging mode with typical tunneling parameters of 1-nA tunneling current and +300-mV tunneling voltage applied to the tip. Variations of the current or voltage did not influence the topography observed by STM.

As target for the ion bombardment a platinum single crystal cut with high precision parallel to the (111) plane has been used. The clean target surface consists of atomically flat terraces of a typical width of 2000 Å separated by monatomic steps.[9,11] The clean sample is prepared by cycles of oxygen exposure ($p_{\text{oxygen}}=2\times10^{-6}$ mbar) and 600-eV Ar^+-ion bombardment both at 800 K followed by annealing to 1250 K.

The ion bombardment has been performed at normal incidence with a differentially pumped ion source with maximum acceleration voltage of 5 keV.[12] The ion beam is scanned to ensure a homogeneous deposition of the ion dose over the entire sample surface. As primary ion species Ne^+, Xe^+, and Ar^+ are used with impurity levels of the gases below 1×10^4 for Ne^+ and Xe^+ or 1×10^5 for Ar^+. The ion current is determined by a Faraday cup, which can be located exactly at the sample position in front of the ion source. The ion energies used are 40 eV, 200 eV, 600 eV, 3 keV, and 5 keV. In the special case of ion bombardment with 40 eV, this low ion energy was achieved by operating the ion source at 200 V acceleration voltage and applying a retarding bias of +160 V to the sample. With the help of a retarding aperture before the Faraday cup entrance hole it was established that the retarding bias of +160 V did not influence the ion flux arriving at the sample. The ion fluxes used are 7.63×10^{15} ions/m^{2}s for Ar^+ and Ne^+ and 6.99×10^{15} ions/m^{2}s for Xe^+. In view of the large yields at high energies, the 5-keV Xe^+ and 5-keV Ar^+ ion fluxes have been reduced to 1.75×10^{15} ions/m^{2}s and 3.82×10^{15} ions/m^{2}s, respectively, to keep the relative error in the duration of the bombardment small. The ion doses ranged from 2.41×10^{16} ions/m^2 for 5-keV Xe^+ to 2.83×10^{19} ions/m^2 for 40-eV Ne^+.

To perform an ion bombardment experiment the clean and well-annealed sample is exposed to the ion beam for a certain time, while the target is at constant temperature. This temperature during ion exposure is named in the following bombardment temperature T_b and is 150 K, if not otherwise specified. When the desired ion dose D is reached the ion bombardment is switched off and the sample is moved—while keeping the temperature at 150 K—to the STM position. After imaging the morphology at 150 K, the sample is successively annealed to higher temperatures $T_a > T_b$. Generally successive 2-min annealing steps at 400 and at 750 K were chosen. Morphologies prepared in this way are indicated for convenience as 150-400-K and 150-400-750-K. After each annealing step the sample is cooled to room temperature (rt) and then imaged to determine the adatom yield Y_a and the sputtering yield Y_s, respectively, as will be discussed in the section below. After the annealing steps, cooling down to rt is sufficient for yield determination, since at this imaging temperature annealed samples show no diffusional changes over hours.

III. ADATOM AND SPUTTERING YIELD-DETERMINATION METHOD

In order to facilitate the presentation of the method and of the associated errors, let us summarize a few facts on the annealing behavior of the defects created by ion bombardment.

A few ten picoseconds after the ion impact, the kinetic energy of the primary ion has been dispersed in the lattice. Relatively stable slower and only thermally decaying defects remain in the impact region (see, e.g., accompanying theoretical paper). These are bulk vacancies, vacancies in the surface layer (surface vacancies), self-interstitial atoms (interstitials), and adatoms on the surface. Especially at higher ion energies in the keV range also agglomerates of surface and bulk vacancies remain in the central cascade region.[13] The formation of interstitial agglomerates, containing more than a few atoms has not been observed so far[14] and seems rather unlikely for ion energies in the keV range. In the case of Pt and the Pt(111) surface, the various defects are mobile for temperatures above 30 K—interstitials,[15] 80 K—adatoms,[16] 180 K—surface vacancies,[17] and 500 K—bulk vacancies.[18] Moreover, for mobile adatoms there is an additional barrier for recombination with surface vacancies and vacancy islands in the surface layer, which is thought to be effective up to 450 K.[2,19]

Figure 1(a) represents the topography obtained after exposing the Pt(111) surface at 150 K to an ion dose of 1.14×10^{18} ions/m^2 of 200-eV Ne^+ ions, which corresponds to the removal of 4.0% of a monolayer (ML) by sputtering. The topography is dominated by small rather irregular adatom islands of monatomic height with a typical length scale of 10 Å. The adatom islands are due to the nucleation of the adatoms generated by the ion impacts. To these adatoms contribute both, atoms transported *athermally* by collisions and replacement collision sequences during the first picoseconds to the surface (energetic contribution) and the atoms transported *thermally* by interstitial migration to the surface (interstitial contribution) on a by far longer time scale. Due to the recombination barrier, the adatoms created at this temperature are relatively stable against recombination with vacancies present at the surface. Thus, most of the generated adatoms condense into adatom islands. In order to avoid the removal of adatoms by subsequent ion impacts, it is important to restrict the ion dose to values corresponding to only a few percent adatom coverage.

At the first glance it is surprising that the morphology of Fig. 1(a) seems to be dominated by adatom islands and not by surface vacancies (mono-, di-, . . . , or islands of vacancies). Only very small dark structures corresponding to surface vacancies are visible. There are two reasons for this. First, the monovacancies created at 150 K by 200-eV Ne^+ bombardment are almost immobile and will thus not form agglomerates larger than a few monovacancies. Due to the finite STM-tip size, small area depressions like surface vacancies are always imaged smaller than they really are. The STM-tip can hardly move into monovacancies or small agglomerates of them. This partially causes the apparent lack of surface vacancies in Fig. 1(a). Generally the area of a depression is reduced by the area of a stripe along its step edge, with a resolution dependent width of the order of 1 Å. Note, that the same effect applies with the opposite sign to adatom islands, i.e., the area of an adatom island is imaged too large by the area of a stripe along the island step edge. Second, the primary ions create many vacancies below the surface which in contrast to the interstitials stay below the surface at 150 K. These bulk vacancies are evidently invisible to STM.

For the other investigated ion energies and species the observed topography after the removal of approximately the same amount of material at 150 K is quite similar. The main difference is that at higher ion energies and larger ion masses the surface vacancies become better visible, despite of the fact that the morphology is still dominated by adatom structures. The reason for this is that at increasingly higher ion energies (or larger ion masses) the surface vacancies are created more and more as agglomerates (craters) of several monovacancies. The large agglomerates are better observable by STM, but still their size is underestimated by the STM-tip effect.

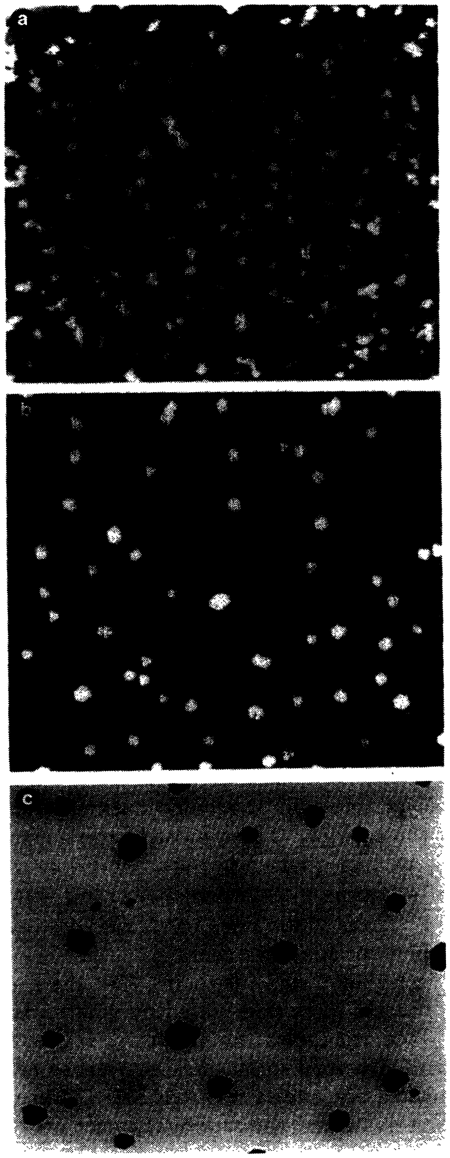

FIG. 1. Annealing sequence of STM topographs after a dose of 1.14×10^{18} ions/m^2 of 200-eV Ne$^+$ at $T_b=150$ K. (a) is imaged directly after bombardment at 150 K (topograph-size 550×480 Å^2, illumination from the left), (b) is a 150-400-K topograph (550×480 Å, gray scale), and (c) is a 150-400-750-K topograph (1100×960 Å^2, gray scale).

The crucial step in the determination of the adatom yield Y_a is the determination of the average fraction X_a of the surface covered by the monolayer high adatom islands. It is evident that this quantity is only meaningful when the analyzed topographs in fact represent almost all generated adatoms in the form of adatom islands. According to the discussion above this condition should be fulfilled for topographs like those in Fig. 1(a). However, due to the small size and even more the roughness and irregular shape of the adatom islands they are imaged—due to the STM-tip effect mentioned above—considerably larger than they are in reality. Image analysis thus would result in an overestimation of the true fraction of a ML covered by adatoms.

To circumvent this problem, the sample is annealed at 400 K resulting in a morphology as shown in Fig. 1(b). The adatom islands have now greatly reduced the length of their boundary step and are compact. Thus the imaging error, which is roughly proportional to the boundary step length is greatly reduced. The adatom islands are bounded by ⟨110⟩ oriented steps and have the appearance of small triangles or hexagons. This island shape with well oriented step directions gives a good criterion for tip quality, allowing us to select only high quality STM topographs for image analysis. Moreover, a coarsening process has taken place, the larger adatom islands having further grown at the expense of the disappearance of the smaller ones. All these changes greatly reduce the error made by estimating X_a via image analysis of STM topographs. Once the value X_a has been determined, the adatom yield is simply

$$Y_a = \frac{X_a \times N_{\mathrm{Pt}}}{D} ,$$

where N_{Pt} is the number of Pt atoms in a ML per m^2 and D is the ion dose per m^2. After the annealing to 400 K not only the adatom islands have become more compact, but also vacancy islands are now clearly visible as dark spots in Fig. 1(b). The improved visibility in comparison to Fig. 1(a) mainly results from the migration and nucleation of the small surface vacancy clusters (monomers, dimers, . . .) to stable immobile vacancy islands.

Annealing to even higher temperatures is detrimental for the correct determination of the adatom yield. It causes a loss of adatoms, which at the higher temperature are no more hindered by the recombination barrier to annihilate with surface vacancies. In addition, when approaching 500-K bulk vacancies start to migrate to the surface where they become either incorporated in a vacancy island or annihilate with an adatom or an adatom island. The decrease in the adatom island covered area is illustrated in Fig. 2. Figure 2(a) is a 150-400-K topograph after 5-keV Xe^+ ion bombardment while Fig. 2(b) is the corresponding 150-400-550-K topograph. Due to the higher annealing temperature the adatom island covered area has decreased whereas the vacancy island covered area has increased substantially in Fig. 2(b) in comparison to Fig. 2(a). The increase in the vacancy covered area demonstrates directly the migration of a large number of bulk vacancies to the surface. Indeed, dissociation of adatom islands and recombination of the resulting adatoms with surface vacancies alone would only have *decreased* the vacancy island covered area. Moreover, the increase of the vacancy island covered area is a proof for the existence of a large number of subsurface vacancies after ion bombardment at $T_b = 150$ K.

The disappearance of adatom islands and the migration of bulk vacancies to the surface at higher annealing temperatures gives the unique opportunity to determine the sputtering yield and the adatom yield in *one* experiment. Figure 1(c) shows a typical 150-400-750-K topograph. Adatom islands are absent on the topograph. During annealing to 750 K the adatom islands dissociated completely into adatoms, which then recombined with surface vacancies. The topograph exhibits only vacancy islands, which are exclusively of monatomic depth with typical lateral dimensions of 50–100 Å. It was carefully checked that the apparent fraction X_s of a ML covered with vacancy islands does not change any more for annealing temperatures from 650 to 850 K.[20] This is a clear indication that in fact all bulk vacancies and vacancy clusters have arrived at the surface after annealing to 750 K. This result is consistent with the annealing behavior of Pt after fast electron irradiation,[21] for which the radiation damage recovers by annealing to 700 K. Consequently, on a 150-400-750-K topograph the missing atoms at the surface—the vacancy islands—represent the sputtered away atoms. The sputtering yield Y_s is then simply

$$Y_s = \frac{X_s \times N_{\mathrm{Pt}}}{D} ,$$

similar to the adatom yield Y_a.

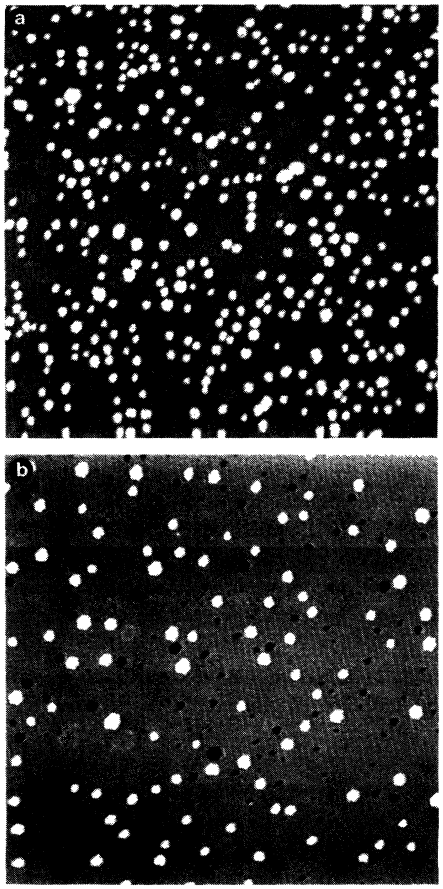

FIG. 2. Gray-scale STM topographs (1100×1100 Å^2) after a dose of 2.41×10^{16} ions/m^2 of 5-keV Xe^+. (a) is a 150-400-K topograph and (b) a 150-400-550-K topograph. In (b) the vacancy island covered area is substantially increased and the adatom island covered area decreased in comparison to (a).

After annealing to 750 K it becomes evident, that a high crystal quality with an extremely low initial step density is a prerequisite for the yield determination method presented here. Figure 3 is a large scale 150-400-750-K topograph (8200×8200 Å^2) after an ion dose of 8.05×10^{16} ions/m^2 of 3-keV Xe^+ ions. It presents a large terrace on which another narrow and elongated terrace (indicated as T in Fig. 3) is present.[22] It is obvious that on both sides of the boundary step of this terrace feature as well as on both sides of the step at the upper edge of the topograph the size and the number of vacancy islands is decreased. In general, all preexisting steps cause such vacancy island denuded zones, which have after annealing for 2 min at 750 K a typical width of 500 Å. Two processes are responsible for the formation of the denuded zones. On the one hand, bulk vacancies ar-

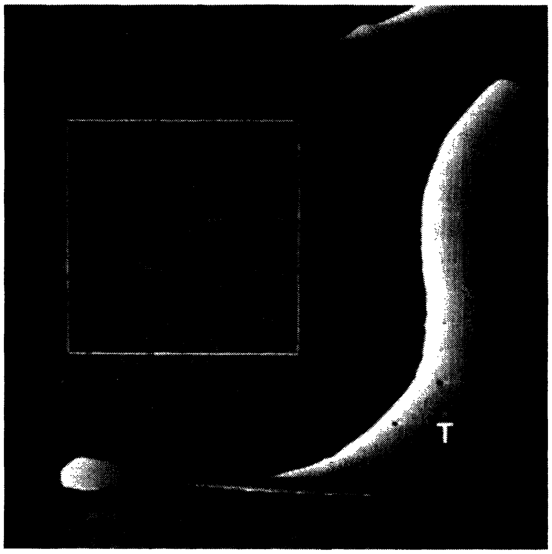

FIG. 3. Large scale 150-400-750-K topograph (8200×8200 Å^2, illumination from the left) of a surface bombarded with a dose of 8.05×10^{16} ions/m^2 3-keV Xe^+ ions. Vacancy island denuded zones are visible on both sides of the boundary step of the large elongated terrace feature T as well as on both sides of the step at the upper edge of the topograph.

riving at the surface close to a preexisting step can anneal at the step edge instead of joining a vacancy island. On the other hand, during the annealing at 750-K atoms become two-dimensional (2D)-evaporated from preexisting step edges. These adatoms move until they recombine with nearby surface vacancies.[23] Such vacancy island denuded zones must be avoided for yield determination purposes. However, areas like those indicated by the square in Fig. 3 are not affected by the preexisting steps and, thus, they represent vacancy island covered areas corresponding to the removed atoms.

In summary, the STM-based methods of adatom yield Y_a and sputtering yield Y_s determination require a precise knowledge of the annealing properties of the ion bombardment defects. Bombardment temperature and annealing steps have to be chosen to fulfill two partially conflicting requirements. On the one hand, the adatom islands after the first annealing step or the vacancy islands after the second annealing step have to represent all adatoms created or all sputtered away atoms, respectively. On the other hand, the islands have to be compact and large enough to keep the errors associated with STM imaging small (moreover, the fractions X_a and X_s should amount at least to a few percent of a ML for the same reason). These requirements may be fulfilled for a variety of metals and different surface orientations, but there may be metals and surface orientations for which this is not possible.

Finally, we want to consider explicitly the errors entering the determination of Y_a and Y_s. As has already become evident from the discussion above, there are three main error sources for the determination of Y_a.

(1) The uncertainty in the knowledge of the ion dose.

(2) The overestimation of the adatom covered area by STM-tip effects.

(3) The underestimation of the number of adatoms generated by using the number of adatoms present in adatom islands as a measure for the adatom yield.

The uncertainty in the knowledge of the ion dose is due to the difficulty to check the precision of the ion current measurement. The adatom yield-determination method has this problem in common with all sputtering yield determination methods. In the present case, however, where the information is obtained from STM images, the actual dose can be checked with superior precision taking advantage of the fact that for ion energies of a few keV each single impact leaves behind a characteristic damage pattern on the surface (see also the discussion in Sec. VI and Fig. 7). For sufficiently low ion doses the damage patterns do not overlap and we are able to check the Faraday cup measurement by comparing its result with the ion dose determined by impact counting. Both values coincide for 5-keV Xe^+-ion bombardment within less than 5%.[24] The overestimation of the adatom covered area due to STM-tip effects [error (2)] could be estimated by comparing typical high-quality topographs with atomic resolution images. However, it was almost impossible to obtain atomic resolution on the rough sputtered surfaces. For image analysis only topographs with sharp island edges have been selected, which typically give the lowest adatom coverages. By a background subtraction and a careful selection of the gray-value threshold, the STM-tip effect was minimized. For small adatom islands with straight step edges on high-quality topographs it is possible to determine the number of adatoms contained in the islands. Comparing this number with the apparent island area the overestimation of the island size due to the STM-tip effect can be assumed to be below 15%. Error (3), the underestimation of the number of generated adatoms by counting the adatom covered area is the biggest problem. The discussion of this error will be separated in three parts. After giving a definition of the ideal adatom yield, the losses of adatoms by nearby impacts, by the imperfection of the recombination barrier and by the annealing process are considered. As mentioned above, the adatoms present on the surface consist of an energetic contribution and an interstitial contribution. The ideal adatom yield as measured by STM here would consist of the number of adatoms present at the surface at the *end* of the energetic phase (when the number of adatoms on the surface is constant on the time scale of picoseconds, see accompanying paper by Gades and Urbassek) plus the adatoms created by interstitial migration to the surface. Note that the ideal adatom yield does not include adatoms being only temporarily present on the surface during the energetic phase. The losses of adatoms already created by nearby impacts are due to the fact, that an adatom may be removed (sputtered or pushed into a vacancy) from the surface by a collision with an energetic atom of another impact. We are unable to give the magnitude of this error. To minimize this error we performed all measurements in the limit of a small dose so that only an adatom coverage of approximately 5% resulted. If the recombination barrier for the recombination of an adatom with a surface vacancy is not perfect, even after the end of the energetic phase single Pt adatom may recombine with a surface vacancy by migration to and subsequent jump into it. Homoepitaxial growth experiments of Pt on Pt(111) by Esch *et al.*[25] directly demonstrated the action of the barrier even at the temperature of 400 K. Recent molecular-dynamics simulations by Villarba and Jonsson[26] confirmed the existence of the step edge barrier. However, the height of the barrier is considerably reduced for rough steps and for such steps recombination events have been observed in the simulation of homoepitaxial growth on Pt(111). We thus only tentatively conclude that the recombination barrier at the much lower temperature of 150 K effectively prevents the adatom-vacancy recombination. Again, we are unable to give quantitatively the magnitude of the leakage of the barrier. Finally, by annealing the sample from 150 to 400 K adatoms may be lost to surface vacancies. By careful comparison of high-quality topographs obtained at 150 K and after annealing to 400 K and by reasonable assumptions on the magnitude of the STM-tip effect we can give an upper bound for this error of 25%. It is quite unsatisfactory that at the moment the total magnitude of error (3) cannot be given. This aspect needs further investigation and we will address this problem in an STM apparatus, which will allow to freeze out the adatom motion. Even though the errors (2) and (3) are systematic, they tend to cancel each other.

Since the uncertainty of error (3) is largest, the adatom yield values determined experimentally have to be considered as a *lower* limit of the real ones. In fact, the measured adatom yields are considerably lower than the adatom yields determined by the molecular-dynamics simulations presented in the accompanying theoretical paper of Gades and Urbassek (see Fig. 6 of their paper). It is compatible with the above error analysis that this deviation may be at least in part due to an experimental underestimation of the true adatom yield. Nevertheless, we want to point out that the errors have roughly the same size and sign for all data points taken. Accordingly, the trends of the energy and ion-mass dependence of the adatom yields thus will be hardly affected.

For the determination of the sputtering yield Y_s a corresponding list applies, the three main error sources being (compare also Ref. 20) the following.

(1) The uncertainty in the knowledge of the ion dose.

(2) The underestimation of the vacancy island covered area by STM-tip effects.

(3) The underestimation of the number of sputtered atoms by using the number of monovacancies present in vacancy islands as a measure for the sputtering yield.

Error (1) needs no further discussion, since it is identical to error (1) in the determination of Y_a. Error (2) is by far smaller than the corresponding error in the adatom island case. After annealing to 750 K the vacancy islands have typical linear dimensions of 30–90 Å [see Fig. 1(c) and also Fig. 3], i.e., they have by far larger areas than the adatom islands with typical linear dimensions of 10–25 Å. The underestimation of the vacancy island area will amount only to a few percent. It could be further reduced by using larger ion doses, causing larger vacancy islands (however, this is not useful for the present experiments, where also the adatom yield is determined). Also, error (3) is smaller and of simpler nature than in the adatom yield case. The losses of vacancies to preexisting steps as well as the filling of surface vacancies by 2D-evaporated atoms from preexisting steps may be neglected in a sufficient distance from these steps. As Fig. 3 demonstrates the crystal quality of our Pt(111) sample allows us to fulfill this condition. The number of atoms sputtered away is underestimated as well, if not all of the subsurface vacancies become annealed at the surface. As mentioned before, from the independence of the vacancy island covered area X_s above annealing temperatures of 650 K[23] and in agreement with the damage annealing in Pt after electron irradiation[21] it can be concluded that the bulk vacancies have almost completely arrived at the surface after annealing to 750 K. Based on the annealing experiments, we estimate the magnitude of this part of error (3) for the presented data to be only a few percent. However, we want to point out the possibility that for even higher bombardment energies in the 10-keV range this might no longer hold. Large vacancy loops, which are still immobile at 750 K might be created at these high energies. Vacancy loop formation has in fact been observed experimentally by Jäger and Merkle[27] for 10-keV Bi^+ bombardment of Au(100).

In conclusion, the sputtering yields presented are considered to be quantitatively correct and the adatom yields to be the lower limits of the true adatom yield, representing correctly their dependence on ion energy and mass.

IV. SPUTTERING YIELDS

The sputtering yield data obtained for Ne^+, Ar^+, and Xe^+ in the energy range from 40 eV to 5 keV are presented in Fig. 4 and Table I. Y_s is ranging over more than three orders of magnitude from 5.2×10^3 for 40-eV Ne^+ to 1.45×10^1 for 5-keV Xe^+ ions. The yields are representative for ion bombardment at normal incidence at $T_b = 150$ K on an atomically flat and clean Pt(111) surface.

The yield depends on the primary ion mass and energy as qualitatively expected form linear cascade theory[28] and as observed previously in experiments with polycrystalline platinum (poly-Pt).[29] For a fixed energy the sputtering yield increases with the mass of the primary ion and for all three gases used the yield increases steeply with energy in the low ion-energy range. However, the maximum, of Y_s for Ne^+ already around 5 keV is surprising. The maximum seems to be shifted to lower energy compared to the expectation from linear cascade theory and measurements for poly-Pt.[29] In addition, the still steep increase of Y_s for Xe^+ from 3 to 5 keV is also surprising. In general, when comparing the yields obtained on Pt(111) with the corresponding poly-Pt data reviewed by Anderson and Bay[29] (some of them are given in the table for comparison) it becomes evident that the Pt(111) values are systematically larger than the poly-Pt ones. For Ar^+ and Xe^+ the deviation clearly increases with ion energy until at 5 keV the single-crystal values exceed the poly-Pt values roughly by a factor of 2.[30]

The situation appears to be similar to the thoroughly investigated case of Ar^+-ion bombardment of Cu(111) and poly-Cu:[31–33] it was found that the Y_s versus energy curve of Cu(111) exhibits (i) a sharper maximum of Y_s, i.e., a steeper increase of the yield with ion energy below the energy of maximum yield and a steeper decrease of the yield for energies above, (ii) a shift of the yield maximum from $\simeq 30$ keV towards lower energies of $\simeq 7$ keV, and (iii) increasingly higher yields up to the energy of the

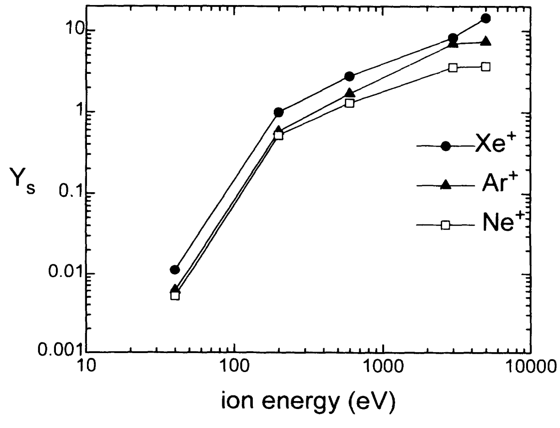

FIG. 4. Sputtering yields Y_s determined by STM for Pt(111) bombardment at $T_b = 150$ K and at normal incidence.

TABLE I. The table gives the sputtering yield Y_s, the adatom yield Y_a, and the ratio Y_a/Y_s for Pt(111) and normal incidence at $T_b = 150$ K in dependence of ion energy and species. Poly-Pt values from the literature (see also Ref. 29) for Y_s are given for comparison.

Ion species	Ion energy	Y_s	Y_s(poly-Pt)	Y_a	Y_a/Y_s
Ne	40	0.0052		0.011	2.1
Ne	200	0.52	0.31 (Ref. 42)	0.45	0.86
Ne	600	1.25	0.70 (Ref. 42)	2.5	2.0
Ne	3000	3.6		5.0	1.4
Ne	5000	3.7		5.1	1.4
Ar	40	0.0061		0.018	2.9
Ar	200	0.58	0.63 (Ref. 42)	0.64	1.1
Ar	600	1.7	1.56 (Ref. 42)	1.3	0.75
Ar	3000	7.0		10.1	1.5
Ar	5000	7.4	3.7 (Ref. 43)	20.5	2.8
Xe	40	0.011		0.10	8.9
Xe	200	1.0	0.72 (Ref. 44)	1.5	1.5
Xe	600	2.8	2.23 (Ref. 44)	4.0	1.4
Xe	3000	8.3		26	3.1
Xe	5000	14.5		66	4.6

maximum yield than in the corresponding curve for poly-Cu. Although it was not possible to measure the yield curves for Pt up to the energies of the maximum yield for Ar^+ and Xe^+, the energy dependence of the sputtering yields of Pt(111) deviates in a similar way from the poly-Pt values as observed formerly for Cu(111) and poly-Cu. Moreover, the sputtering yield curves presented here for Ne^+- and Xe^+-ion bombardment on Pt(111) are qualitatively similar to the curves obtained by Szymczak and Wittmaack[34] for Ne^+- and Xe^+-ion bombardment on Au(111). The two sets of curves are even quantitatively almost identical. The molecular-dynamics simulations presented in the accompanying paper also show reasonable agreement with the sputtering yields determined here. All these facts suggest, that the STM based method allows for reliable sputtering yield determination. The STM yield-determination method is inherently a low dose method and allows us to attack some of the remaining problems in sputtering, e.g., the morphology dependence of the yield and closely related to this the dose dependence of the yield.[20]

V. ADATOM YIELDS

Figure 5 and Table I present the adatom yield data obtained after bombardment at $T_b = 150$ K with the same ion species and in the same energy range as for the sputtering yield data. The Y_a-data exhibit the following characteristics: (i) the adatom yields are typically larger than the sputtering yields (see also Fig. 6). They range from 1.1×10^2 for 40-eV Ne^+ to 6.6×10^1 for 5-keV Xe^+. (ii) For a fixed ion energy an increase of Y_a with the mass of the primary ion is observed, similar to Y_s. However, there is an exception at 600 eV, where Y_a for Ne^+ is larger than the yield for Ar^+. (iii) The adatom yield increases steeply in the low-energy region, but the increase between 40 and 200 eV is not as strong as for the corresponding sputtering yields. (iv) Whereas Y_a for Ne^+ already seems to approach its maximum value around 5 keV, Y_a increases *strongly* above 600 eV for Ar^+ and Xe^+.

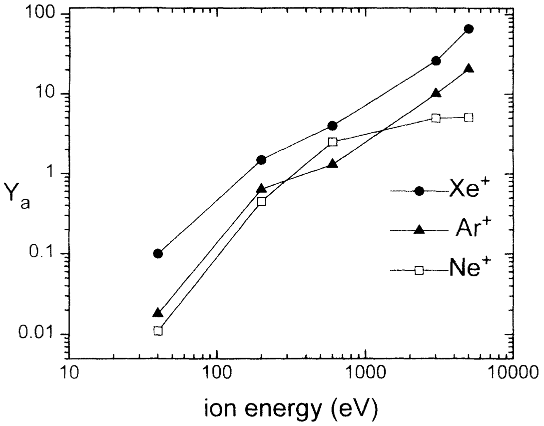

FIG. 5. Adatom yields Y_a determined by STM for Pt(111) bombarded at $T_b = 150$ K and at normal incidence.

What dependence on ion energy and on ion mass should one expect for the adatom yields? Based on previous theoretical and calculational approaches we find the following answers to this question.

(1) According to the sputtering theory of Sigmund,[28] Robinson[35] states that "In a structureless medium, approximately one half of the particle incident on the surface barrier are actually sputtered." Assuming that a particle incident on the surface barrier not being sputtered becomes an adatom, linear cascade theory predicts a ratio $Y_a/Y_s \simeq 1$ independent of the primary ion energy and the ion mass.

(2) TRIM (Ref. 36) calculations performed for various ion species and energies give the same result: the number of particles approaching the surface barrier is approximately twice the number of particles sputtered, i.e., $Y_a/Y_s \simeq 1$.

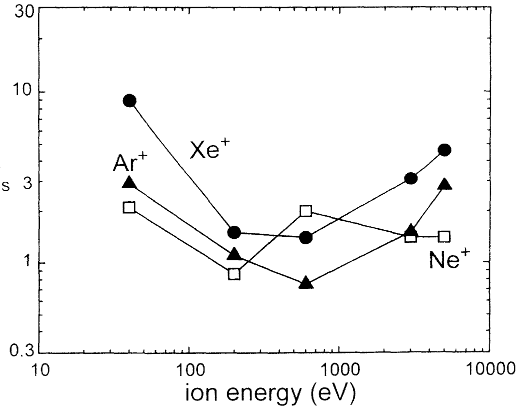

FIG. 6. Ratio of the adatom yield to the sputtering yield Y_a/Y_s for the data of Figs. 4 and 5.

(3) Based on molecular-dynamics simulations of Ar^+-ion bombardment on Cu(100) Webb and Harrison[1] postulated that "Approximately, the number of target adatoms created equals the number of adatoms sputtered. This general principle holds for most impact points and energies to date. At lower energies (~ 1 keV) the ratio of target adatoms to sputtered atoms tends to decrease." In conclusion, $Y_a/Y_s \simeq 1$ for energies, >1 keV, again independent of ion energy and ion mass, and a tendency for $Y_a/Y_s < 1$ at energies <1 keV.

In view of the limitations of the applied concepts, the answers should hold for ion energies in the keV range. It is surprising, how these concepts agree in their prediction of the yield ratio $Y_a/Y_s \simeq 1$. It is even more surprising that in comparison to the experimental data all three concepts clearly fail.

The experimental yield ratios Y_a/Y_s are present in Fig. 6 and Table I. They show that (1) the highest yield ratio for all three ion species is obtained for the lowest investigated ion energy of 40 eV ranging from 2.1 to 8.9. (2) The theoretical prediction of $Y_a/Y_s \simeq 1$ is close to the lower limit of all experimental ratios. (3) For Ar^+ and Xe^+ a clear minimum around 600 eV is present. For higher ion energies their yield ratios increase again, whereas for Ne^+ the ion-energy dependence is weak. (4) Except for the 600-eV Ne^+ data point the rule holds: the higher the primary ion mass, the greater the ratio Y_a/Y_s. In conclusion, the yield ratios exhibit a pronounced dependence on both the ion energy and the mass of the primary ion.

In the following, the origin of the behavior of Y_a/Y_s will be discussed qualitatively. First, the origin of the high ratios at 40 eV is briefly considered. In contrast to a sputtered atom, an adatom is still bound to the surface. Consequently, creation of an adatom needs less collisional energy than sputtering an atom. In other words, the threshold energy of the primary ion for creating an adatom is lower than for creating a sputtered atom. Thus, the lowering of the primary ion energy, in an energy range where a sputtering event is already rare, will reduce the number of atoms sputtered to a greater extent, than the number of atoms becoming adatoms. This gives rise to a steeper decrease of the sputtering yield and consequently large numbers of Y_a/Y_s. A full analysis of the origin of the high yield ratios at low energies, which is in agreement with the simplified picture presented here, is given in the accompanying theoretical paper by Urbassek and Gades. Profound consequences for ion-beam assisted deposition may be inferred from the observation of the high yield ratios at very low energies: at ion energies <100 eV the ion beam creates additional diffusing species—surface vacancies and the more mobile adatoms in equal numbers—while the amount of sputtered atoms is very low.

Let us now consider the origin of the increase of the yield ratios for Ar^+ and Xe^+ in the keV range. As already pointed out in Sec. III the adatom yield consists of the energetic contribution of the adatoms present at the surface after the end of the energetic phase and of the interstitial contribution due to interstitial migration to the surface. Experimentally it would only be possible to separate these two contributions by performing ion bombardment experiments at temperatures low enough to freeze out interstitial migration. The interstitial contribution is not included in any of the adatom yields of the theoretical answers above. Thus, one might suspect that the experimentally observed increase of the yield ratio Y_a/Y_s at higher ion energies for Ar^+ and Xe^+ is due to the increasing magnitude of the interstitial contribution to the experimentally determined adatom yields. This could then explain the difference between the theoretical yield ratios $Y_a/Y_s \simeq 1$ and the larger experimental ones. However, this reasoning fails as the following estimates show. An upper bound for the number of interstitials created by a primary knock on atom (PKA) of 5 keV in bulk Pt can be estimated to be 35 using the modified Kinchin-Pease approximation of Norget, Robinson, and Torrens (NRT)[37] and by taking into account the orientational dependence of the damage threshold for Pt.[38] After subtracting this number from the experimental adatom yield for 5-keV Xe^+ still a ratio $Y_a/Y_s > 2$ results for this energy and ion species. In addition, the interstitial contribution could not cause the strong increase of Y_a between 3 and 5 keV for Ar^+ and Xe^+ (Y_a increases from 26–66 for Xe^+). Moreover, the interstitial contribution to the adatom yield is largely overestimated by the use of the NRT approximation due to following reasons. (1) Moleculear dynamics simulations of 5-keV PKA events in Cu- and Ni-bulk by Diaz de la Rubia *et al.*[39] systematically yield less interstitials than would be expected from the NRT approximation, indicating a general overestimation of the interstitials created by use of the NRT approximation. (2) The NRT approximation is based on the assumption, that the PKA's are initiated in the bulk. However, in our case the PKA's are initiated near the surface. Thus energetic atoms will move towards the empty half space above the surface and may become adatoms or sputtered atoms. In the bulk case, where no empty half space exists at least some of these atoms would have become interstitials. (3) At the temperatures under consideration, which allow interstitial migration, it has to be expected that a considerable number of interstitials recombine with bulk vacancies before they reach the surface. (4) As will be discussed in more detail in the following section on single ion impacts, for 5-keV Xe^+ an average of 5.5 extra atoms per impact is found *in* the surface layer in a reconstruction loop and not *on* the surface. These extra atoms may be assumed to result from interstitial migration into the surface layer.[7] In conclusion, the possible interstitial contribution to the adatom yield on the surface layer decreases to something like five interstitials per 5-keV Xe^+ impact, and is even less for the other ion species and energies. The interstitial contribution contained in the experimentally determined adatom yields thus cannot account for deviations in the keV range of the experimental Y_a/Y_s values from the theoretically expected value $Y_a/Y_s \simeq 1$.

A speculative explanation of the origin of the increase of the yield ratios of Ar^+ and Xe^+ with ion energy is the possible onset of nonlinear or spike effects. In fact, for 3-keV Xe^+-ion bombardment the molecular-dynamics simulations presented in the accompanying paper of

Gades and Urbassek indicate the presence of a collisional spike. Recent molecular-dynamics simulations of collision cascades initiated by 10-keV Au^+ impacts on Au performed by Ghaly and Averback[6] indicate the development of a molten area reaching the surface during the evolution of the spike. Due to the thermal expansion of the liquid droplet a considerable amount of material is observed to flow onto the surface where it recrystallizes. Such spike effects could cause a considerable increase in the adatom yield and might also play a role for keV ion bombardment on Pt(111). This is supported by the occasional observation of "large" impact events with up to 500 atoms pushed onto the original surface layer[7] after 5-keV xenon bombardment. Spike effects are expected to be more pronounced for heavier ions which deposit their energy in a smaller volume and thus allow the necessary energy density for spike formation to be achieved. In the case of keV Ne^+-ion impacts the necessary energy density is not reached, and thus the yield ratio does not increase with ion energy, as observed. Finally, we want to remark that the increasing energy density in the impact region due to the increased ion energy might affect the adatom yield already below the spike threshold.

In summary, the ratio of adatom to sputtering yield exhibits a substantial dependence on ion mass and energy, in contrast to previous theoretical and calculational expectations. The high yield ratios observed for 40-eV, Ne^+-, Ar^+-, and Xe^+-ion bombardment are a threshold effect, whereas the large yield ratios in the keV range for Ar^+ and Xe^+ are possibly indicative for spike effects.

VI. SINGLE-ION IMPACTS

During the experiments for adatom and sputtering yield determination, it was discovered that the damage pattern of *individual* ion impacts on a metal may be recognized in detail by STM.[7] In the case of Pt(111), this appears to be possible even at ambient temperature ion bombardment for ion energies of a few keV. The lowest energy at which single-ion impacts can be detected is temperature dependent. For low target temperatures where surface diffusion is completely prevented, single-ion impacts in the eV range should also be detectable. Figure 7 represents the surface morphology after a dose of 4.1×10^{16} ions/m^2 of 5-keV Xe^+ ions at 300 K, corresponding to an average of 24 impacts on an area of the size of the topograph shown. Each impact causes a damaged area with linear dimensions of less than 100 Å, typically of 50 Å. As mentioned before, in a number of bombardment experiments with ion doses between $(0.75-4.1)\times10^{15}$ ions/m^2 it was always found that the number of visible defected areas coincides within 5% with the number impacts to be expected from the Faraday cup measurements. Three distinct damage features contained in the damaged areas can clearly be distinguished: vacancy islands (craters), adatom islands of monatomic height, and ringlike to triangular corrugation line features with a height of 0.2 Å (for convenience called loops). A typical defected area consists of a crater and one of the following configurations: (1) one or several adatom islands, (2) a loop and one or several adatom islands, or (3) a loop only. Sometimes even larger more structured corrugation line features are found in between several impact craters (see 4 in Fig. 7) and occasionally also loops further away from defected areas are observed (5 in Fig. 7). In general, the lateral correlation between loops and impact craters is somewhat weaker than between the adatom islands and the craters.

If we assume that the craters are bounded by {111} facets, which are the steepest possible crater walls without overhangs, they contain an average between 10 and 20 vacancies. The sputtering yield of 5-keV Xe^+ ions is 14.5. The craters are thus roughly the size that would result from the sputtered away atoms alone. The observation has the implication that most of the vacancies compensating for the adatoms on the surface have still to be found below the surface. This is in agreement with the annealing experiments described in III (see also Fig. 2), which already proved the existence of a large number of subsurface vacancies after ion bombardment at 150 K. The correlation between sputtering yield and visible vacancies requires that at the given bombardment temperature the adatoms created are unable to fill in the surface vacancies and the bulk vacancies created are unable to migrate to the surface. These conditions are expected to be still fulfilled at 300 K, at which temperature bombardment in Fig. 7 was performed. A similar correlation between surface vacancies and sputtering yield was found in a field-ion microscopy (FIM) investigation of 20-keV Kr^+ irradiation on a Pt-tip by Pramanik and Seidmann.[13] Also a large number of subsurface vacancies was detected in accord with our observations. The fate of the atoms kicked out in order to create the subsurface vacancies, however, could not be established in that study.

The number of adatom islands associated with an impact crater varies between 0 and 4 at $T_b = 300$ K, and can

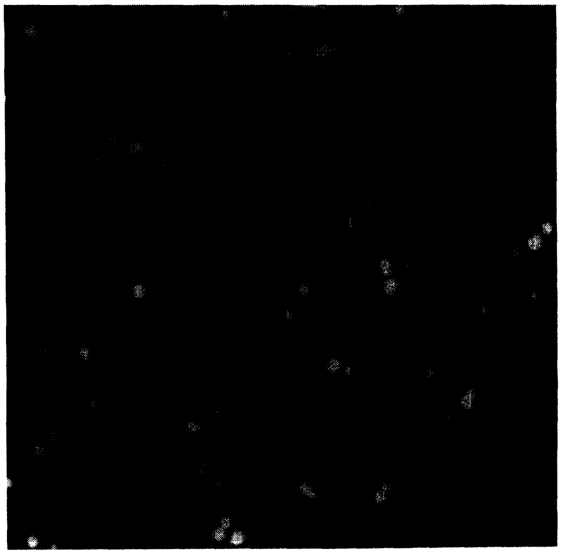

FIG. 7. STM topograph (770×770 Å^2, illumination from the left) of single-ion impacts on Pt(111) obtained after a dose of 4.1×10^{15} ions/m^2 of 5-keV Xe^+ at $T_b = 300$ K. The defect patterns 1–6 are discussed in the text.

be as high as 7 at $T_b = 150$ K. If there is more than one adatom island associated with one impact crater, the impact crater is found between the islands. The adatom islands *surround* the impact crater. The same holds for combinations of loops and adatom islands. The crater is almost exclusively found between the different damage features. This arrangement in fact indicates that the craters are positioned at the impact point (not more than a few angstroms away from it) and the other damage features are created further away from it in a typical separation of 20–30 Å. The lateral distribution of the damage observed by STM at the surface corresponds well to the FIM experiments of Seidmann, Averback, and Benedek.[14] There, the formation of a vacancy rich core with vacancy clusters is observed together with a zone of increased atomic density (interstitials) surrounding it. A similar distribution of damage is also simulated for keV cascades in metal bulk.[39]

Note, however, that the damage patterns of energetic ion impacts scatter considerably. This has already been concluded from the scatter of the number and distribution of bulk vacancies as analyzed by FIM.[13] The present data give a drastic illustration of this scatter, too. Not only the crater size varies, but even more obvious does the number of adatoms created per impact. In event 3 of Fig. 7 no adatoms are created, in event 6, around 200 adatoms were created. Events with up to 500 adatoms created by a single impact have been observed.[7]

The loop features present in Fig. 7 have been discussed in detail in Ref. 7. Briefly, the Pt(111) surface layer has a natural tendency (due to the existence of tensile surface excess stress) to decrease the Pt-Pt bond length by insertion of extra atoms.[40] Manifestations of this tendency are the formation of an equilibrium reconstructed surface phase above 1330 K (Ref. 41) and of a metastable reconstructed surface phase which an be created above 400 K in the presence of a supersaturated Pt vapor.[42,45] Both reconstructed phases exhibit an atomic surface density increased by a few percent in comparison to the unreconstructed surface. The loop features observable in Fig. 7 are again a consequence of the tendency of Pt(111) to reconstruct. They are created by insertion of an average of 18±5 extra atoms per loop into the surface layer after 5-keV Xe^+ bombardment. The interior of the loop has hcp stacking, the exterior evidently fcc stacking, and the bright corrugation line is a transition area which accommodates the extra atoms. It has been demonstrated experimentally that the loops created upon ion impact are in fact identical to the nuclei of the metastable reconstruction surface phase of Pt.[7] The ion impact induced interstitials, which migrate to the surface, are trapped with high efficiency in the surface layer and create these loops even at temperatures as low as 150 K. However, it is still an open question, to what extent collective effects contribute to loop formation. Dedicated molecular-dynamics simulations could probably answer it. For the special case of surfaces with substantial tensile stress like Pt(111) not only the sputtering yield and adatom yield may be determined experimentally, but also the surface interstitial yield. This surface interstitial yield is defined as the number of extra atoms created *in* the surface layer per ion impact. For Xe^+ ions it starts to deviate from 0 already at 400 eV and reaches a value as high as 5.5 at 5 keV.

In this last section of the paper, it has been demonstrated that by STM detailed images of the complex damage patterns of single-ion impacts are obtained. For 5-keV Xe^+ bombardment one crater per impact is visible, which is surrounded by a number of adatom islands containing between zero and up to 500 adatoms and also by loop features characteristic so far only for the Pt(111) surface. Comparison of molecular-dynamics simulations with the real-space damage distributions obtained by STM might be of great help for getting a deeper insight into the processes determining the ion-surface interaction.

ACKNOWLEDGMENTS

The authors acknowledge the critical reading of the manuscript by George Comsa, Uffe Littmark, Herbert Urbassek, Markus Morgenstern, Stefanie Esch, and Mark Reuter, which helped to improve the paper considerably, the help of Uffe Littmark who performed the TRIM calculations and the constructive collaboration with Heinrich Gades and Herbert Urbassek. The discussions on the issue with the persons mentiond above as well as Michael Hohage and Bob Averback helped to shape the ideas presented here. One of us (C.T.) acknowledges support from the Alfried Krupp von Bohlen und Halbach Foundation and support from the Alexander von Humboldt Foundation.

---

[*] Present address: University of Wisconsin-Madison, Engineering Research Building, 1500 Johnson Drive, Madison, Wisconsin 53706.

[1] R. P. Webb and D. E. Harrison, Jr., Radiat. Eff. Lett. **86**, 15 (1983).

[2] Th. Michely and George Comsa, Phys. Rev. B **44**, 8411 (1991).

[3] M. Breemann and D. O. Boerma, Surf. Sci. Lett. **278**, L110 (1992).

[4] J. C. Girard, Y. Samson, S. Gauthier, S. Rousset, and J. Klein, Surf. Sci. **302**, 73 (1994).

[5] F. Karetta and H. M. Urbassek, J. Appl. Phys. **71**, 5410 (1992).

[6] M. Ghaly and R. S. Averback, Phys. Rev. Lett. **72**, 364 (1994).

[7] C. Teichert, M. Hohage, Th. Michely, and G. Comsa, Phys. Rev. Lett. **72**, 1682 (1994).

[8] F. A. Smidt, Int. Mat. Rev. **35**, 61 (1990).

[9] Th. Michely, Ph.D. thesis, Forschungszentrum Jülich, Jülich, 1991.

[10] K. H. Besocke, Surf. Sci. **181**, 145 (1987); Th. Michely, K. H. Besocke, and M. Teske, J. Microsc. **152**, 77 (1988); J. Frohn, J. F. Wolf, K. H. Besocke, and M. Teske, Rev. Sci. Instrum.

60, 1200 (1989).

[11] U. Linke and B. Poelsema, J. Phys. E **18**, 26 (1985).

[12] Ion source IQE 12/38 manufactured by SPECS GmbH, Berlin.

[13] D. Pramanik and D. N. Seidmann, J. Appl. Phys. **60**, 137 (1986).

[14] D. N. Seidmann, R. S. Averback, and R. Benedek, Phys. Status Solidi B **44**, 85 (1987).

[15] H. J. Dibbert, K. Sonnenberg, W. Schilling, and U. Dedek, Radiat. Eff. **15**, 115 (1972).

[16] D. W. Basset and P. R. Webber, Surf. Sci. **70**, 520 (1978).

[17] B. Poelsema, K. Lenz, R. S. Brown, L. K. Verheij, and G. Comsa, Surf. Sci. **162**, 1011 (1985).

[18] K. Sonnenberg, W. Schilling, K. Mikka, and K. Dettmann, Radiat. Eff. **16**, 65 (1972).

[19] R. Kunkel, B. Poelsema, L. K. Verheij, and G. Comsa, Phys. Rev. Lett. **65**, 733 (1990).

[20] Th. Michely, G. Comsa, Nucl. Instrum. Methods Phys. Res. Sect. B **82**, 207 (1993).

[21] P. Ehrhardt, in *Atomare Fehlstellen in Metallen,* edited by H. Ullmaier, Landolt-Börnstein, New Series, Group III, Vol. 25 (Springer, Berlin, 1991), p. 256ff.

[22] Features like this are occasionally found on terraces in excess of 5000-Å width. The last annealing cycle of 10*s* duration at 1250 K *before* the ion bombardment experiment was not sufficient to dissociate such structures.

[23] Th. Michely, T. A. Land, U. Littmark, and G. Comsa, Surf. Sci. **272**, 204 (1992).

[24] The method of impact counting gives the unique opportunity to calibrate Faraday cups.

[25] S. Esch, M. Hohage, Th. Michely, and G. Comsa, Phys. Rev. Lett. **72**, 518 (1994).

[26] M. Villarba and H. Jonsson, Phys. Rev. B **49**, 2208 (1994).

[27] W. Jäger and K. L. Merkle, Philos. Mag. A **57**, 479 (1988).

[28] P. Sigmund, Phys. Rev. **184**, 383 (1968).

[29] H. H. Anderson and H. L. Bay, in *Sputtering by Particle Bombardment,* edited by R. Behrisch (Springer, Berlin 1981), Vol. 1, p. 145.

[30] The sputtering yield of 14.5 for 5-keV Xe^+-ion bombardment seems to be one of the highest yields measured on a metal at this energy.

[31] H. E. Roosendaal, in *Sputtering by Particle Bombardment* (Ref. 29), p. 219.

[32] T. W. Snouse and L. C. Haughney, J. Appl. Phys. **37**, 700 (1966).

[33] D. Onderlinden, Appl. Phys. Lett. **8**, 189 (1966).

[34] W. Szymczak and K. Wittmaack, Nucl. Instrum. Methods Phys. Res. **194**, 561 (1982).

[35] M. T. Robinson, in *Sputtering by Particle Bombardment* (Ref. 29), p. 81.

[36] J. F. Ziegler, TRIM-93, IBM Research Division, T. J. Watson Research Center, P.O. Box 218, Yorktown Heights, New York.

[37] W. Schilling and H. Ullmaier, in *Physics of Radiation Damage in Metals,* edited by R. W. Cahn, P. Haasen, and K. Kramer, Materials Science and Technology Vol. 10 (Verlag Chemie, Weinheim, 1993).

[38] P. Jung, R. L. Chaplin, H. J. Fenzl, K. Reichelt, and P. Wombacher, Phys. Rev. B **8**, 553 (1973).

[39] T. Diaz de la Rubia, R. S. Averback, Horngming Hsieh, and R. Benedek, J. Mater. Res. **4**, 579 (1989).

[40] R. J. Needs, M. J. Godfrey, and M. Mansfield, Surf. Sci. **242**, 215 (1991).

[41] A. R. Sandy, S. G. J. Mochrie, D. M. Zehner, G. Grübel, K. G. Huang, and D. Gibbs, Phys. Rev. Lett. **68**, 2192 (1992).

[42] M. Bott, M. Hohage, Th. Michely, and G. Comsa, Phys. Rev. Lett. **70**, 1489 (1993).

[43] N. Laegreid and G. K. Wehner, in *1960 National Symposium on Vacuum Technology Transactions,* edited by R. Meisner (Pergamon, New York, 1961), p. 286.

[44] H. Schirrwitz, Beitr. Plasmaphys. **2**, 188 (1962).

[45] D. Rosenberg and G. K. Wehner, J. Appl. Phys. **33**, 1842 (1962).

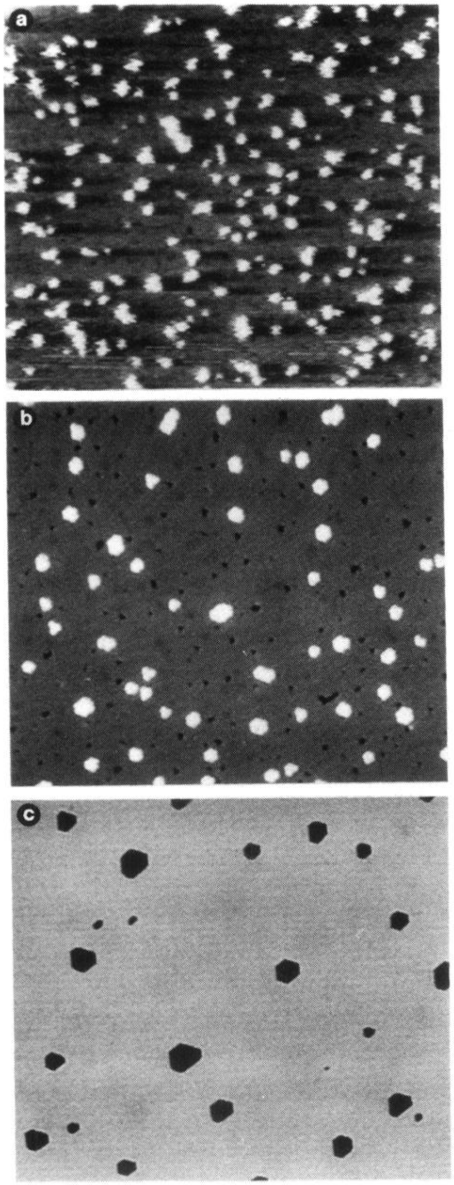

FIG. 1. Annealing sequence of STM topographs after a dose of 1.14×10^{18} ions/m^2 of 200-eV Ne$^+$ at $T_b = 150$ K. (a) is imaged directly after bombardment at 150 K (topograph-size 550×480 Å^2, illumination from the left), (b) is a 150-400-K topograph (550×480 Å, gray scale), and (c) is a 150-400-750-K topograph (1100×960 Å^2, gray scale).

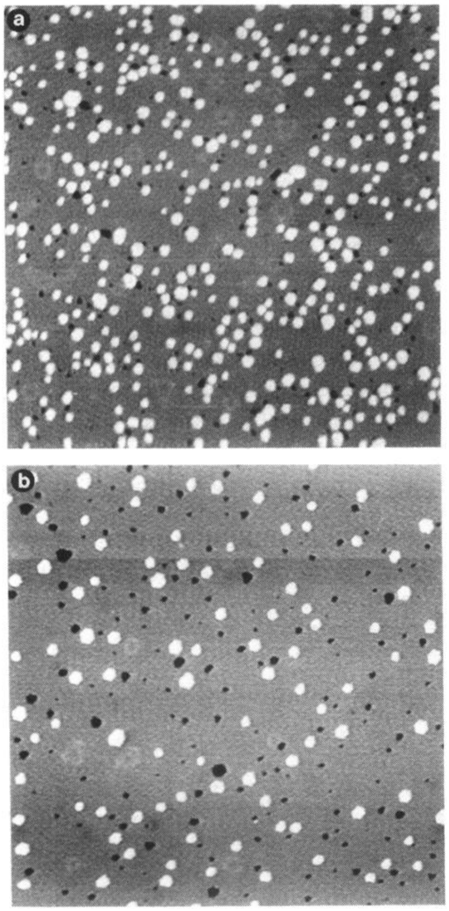

FIG. 2. Gray-scale STM topographs (1100×1100 Å^2) after a dose of 2.41×10^{16} ions/m^2 of 5-keV Xe$^+$. (a) is a 150-400-K topograph and (b) a 150-400-550-K topograph. In (b) the vacancy island covered area is substantially increased and the adatom island covered area decreased in comparison to (a).

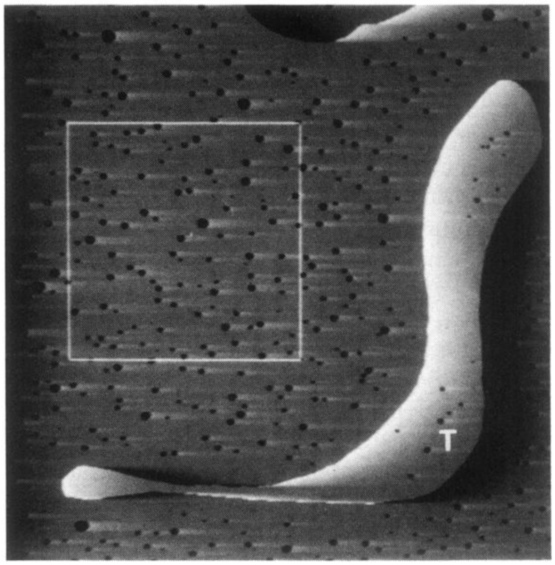

FIG. 3. Large scale 150-400-750-K topograph (8200×8200 Å^2, illumination from the left) of a surface bombarded with a dose of 8.05×10^{16} ions/m^2 3-keV Xe$^+$ ions. Vacancy island denuded zones are visible on both sides of the boundary step of the large elongated terrace feature *T* as well as on both sides of the step at the upper edge of the topograph.

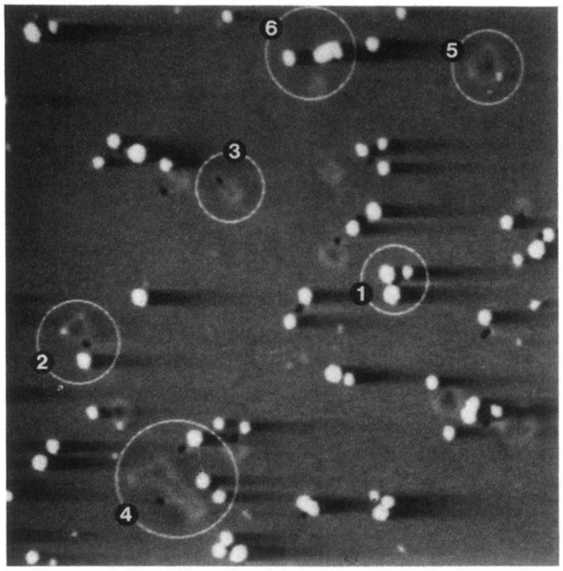

FIG. 7. STM topograph (770×770 Å^2, illumination from the left) of single-ion impacts on Pt(111) obtained after a dose of 4.1×10^{15} ions/m^2 of 5-keV Xe$^+$ at $T_b=300$ K. The defect patterns 1–6 are discussed in the text.